

# Carbon Membranes for High Temperature Gas Separations: Experiment and Theory

Gabriel A. Szejner, Irena Efremenko and Moshe Sheintuch

Dept. of Chemical Engineering, Technion - Israel Institute of Technology, Haifa 32000, Israel

*The transport and separation of hydrogen and light alkanes are studied in a molecular-sieve carbon membrane hollow-fiber module at the temperature range of 25–400°C; nitrogen is used as a sweeping gas in the study of mixtures, and the fluxes of pure components are studied under a pressure gradient. The membrane selectivity, the ratio of hydrogen to hydrocarbon permeabilities, may reach 100 to 1,000 in propane, or in (normal or iso-) butane mixtures with hydrogen, making the membrane an excellent candidate for a membrane dehydrogenation reactor. The permeabilities measured in pure-component studies differ from those in mixtures. Specifically, counterdiffusion of nitrogen and C<sub>2</sub> to C<sub>4</sub> alkanes significantly inhibits the fluxes of both, whereas the hydrogen flux is only slightly diminished. To account for these results, molecular mechanics simulations are used to find the energetics of adsorption, diffusion, and desorption of individual gases in cylindrical nanopores modeled by carbon nanotubes. In pore sizes that are up to 2–3 times the dimension of the molecule, diffusion of the molecule inside the pore is nonactivated, whereas desorption is activated and typically is the rate limiting step; the molecular transport proceeds essentially by the single-file diffusion mechanism. A rate expression for a single-species transport in a molecular-sieve carbon membrane is derived by a mean-field approach. The pore-size distribution calculated by comparing experimental and computed fluxes favorably compares with the measured distribution.*

© 2004 American Institute of Chemical Engineers *AIChE J.* 50: 596–610, 2004

**Keywords:** molecular sieves, carbon membrane, carbon nanotube, molecular transport and separation

## Introduction

Transport of gas mixtures through inorganic membranes is the subject of great current interest (Keil, 1996, 1999). Although, inorganic membranes can withstand high temperatures, issues, such as membrane mechanical instability (embrittlement), insufficient permeability or permselectivity, or simply high costs, still hamper the application of inorganic membranes in the process industry (Saracco and Specchia, 1998). Dense metal membranes (Pd, Ag, including their alloys) or solid electrolytes allow for selective diffusion of hydrogen or oxygen. Transport in dense membranes occurs by dissolution of

the molecules in the membrane, followed by diffusion of the molecules (or ions in solid electrolytes), and desorption (Uhlhorn, 1991). Dense membranes are usually too expensive for commercial applications, and show high selectivity but low permeability. Porous membranes consist of a highly porous metal, or a ceramic support with a thin top layer tailored to have the desired selectivity (Burggraaf, 1991), yield quite a high permeability, but a relatively low selectivity.

In a search for a highly selective and relatively inexpensive membrane, that may be employed in membrane reactors for the separation of hydrogen simultaneously with equilibrium-limited reaction, the separation of hydrogen and hydrocarbons in carbon membranes are studied. Carbon membranes are molecular sieves that incorporate pores of molecular dimensions, so that steric and other effects associated with the proximity of the pore wall play an increasingly important role in transport

Correspondence concerning this article should be addressed to M. Sheintuch at [cermsll@tx.technion.ac.il](mailto:cermsll@tx.technion.ac.il).

processes. Another selection mechanism that is important at relatively low temperatures is due to adsorption and surface diffusion. Because the interest is in high-temperature applications, the study of separation is in the range of 25–500°C. This work describes the separation selectivities of a mixture of hydrogen and hydrocarbons, and attempt to explain them in terms of kinetic models, with energies calculated by molecular mechanics modeling.

### Membrane preparation

Molecular sieve carbons (MSC) can be prepared by the pyrolysis of thermosetting polymers, such as polyvinylidene chloride, polyfurfuryl alcohol, cellulose triacetate, polyacrylonitrile, and phenol formaldehyde (Bird and Trim, 1983). A different approach, involving a polymeric system such as polyacrylonitrile (PAN) in a hollow fiber configuration, followed by pyrolysis in an inert atmosphere, was suggested by Koresh and Soffer, (1980, 1986, 1987). An oxidation treatment is then necessary to create a permeable pore structure; the oxidation treatment determines the pore sizes and the identity of the molecules that can be absorbed, and thus transported, through the system.

Ultramicroporosity was obtained by Koresh and Soffer (1983) after thermal treatment in a vacuum, and this was the basis for the development of a hollow-fiber gas-separation membrane. This ultramicroporosity is because of small gaseous molecules channeling their way out of the solid matrix during pyrolysis. These micropores can be opened up by further activation (oxidation at moderate temperatures, 400–500°C), or closed by high-temperature sintering. The pore opening by a high-temperature evacuation is because of the removal of surface oxygen groups such as CO<sub>2</sub> and CO. The fact that it essentially terminates at ≈ 400°C, suggests that at higher temperatures, where surface groups can still be degassed as CO, sintering may already have taken place.

### Transport selectivity

Adsorption tests show that the pore structure is composed from relatively wide pores, separated by a few constrictions responsible for the molecular sieving effect (Koresh and Soffer, 1980). Koresh and Soffer (1987) tested the permeation of a H<sub>2</sub>/CH<sub>4</sub> mixture, and found that, even at low temperatures where considerable adsorption is very likely, H<sub>2</sub> permeabilities are independent on mixture composition. Rao and Sircar (1993) tested the permeation of hydrogen and C<sub>1</sub>–C<sub>4</sub> hydrocarbons through a flat supported carbon membrane at 296 K. All pure-gas hydrocarbons were found to have larger permeabilities than H<sub>2</sub>, because of their preferential adsorption on the carbon surface compared to H<sub>2</sub>. The permeabilities increased from H<sub>2</sub> to CH<sub>4</sub> to C<sub>2</sub>H<sub>6</sub>. Then, they progressively decreased as the molecular weight of the hydrocarbon chain increased. This behavior is consistent with the observation that the specific adsorbed amount of hydrocarbons in the carbon pores increases as the hydrocarbon molecular weight increases; however, the strength of adsorption also increases, causing the higher hydrocarbons to be less mobile on the surface. In a mixture, the permeabilities of the most weakly adsorbed components are drastically reduced in the presence of the higher hydrocarbons. The same results were achieved with a tubular supported car-

bon membrane at 296 K (Sircar et al., 1999). Sircar et al. (1999) also tested the carbon dioxide–methane–hydrogen system, finding that CO<sub>2</sub> and CH<sub>4</sub> are preferentially permeated through the membrane at room temperature. Kusuki et al. (1997) found that in the temperature range of 25–120°C, the permeability of light alkanes decreased with the kinetic diameter of the gas and, hence, the permeability of each gas increased with the temperature. Tanihara et al. (1999) tested the permeation of H<sub>2</sub>, CO<sub>2</sub> and CH<sub>4</sub> in a carbon hollow fiber membrane, prepared by pyrolyzing an asymmetric polyimide hollow fiber membrane. They found a selectivity factor of 540 in a mixture of H<sub>2</sub>/CH<sub>4</sub> at 50°C.

### Transport mechanisms

Determining the mechanism responsible for flow and separation of multicomponent molecular mixtures through nanoporous materials is a challenging experimental task (Weitkamp et al., 1991; Chen et al., 1994; Xu et al., 1999; Mao and Sinnott, 2000, 2001), because it is nontrivial to produce nanoporous materials of known average pore sizes, and of identified distributions. The understanding of the transport and separation phenomena in carbon membranes is still largely incomplete (Duren and Keil, 2001), because transport mechanisms vary with the pore size, the pore network structure, and the molecule size and shape, along with the interaction between the transported species and membrane material. Transport mechanisms inside the pores of a membrane are usually classified into the following: (a) viscous flow, (b) Knudsen diffusion, (c) surface diffusion, (d) multilayer diffusion, (e) capillary condensation, and (f) molecular sieving (Saracco and Specchia, 1994). Viscous flow and molecular diffusion do not apply for nanopores of molecular size. Knudsen diffusion leads to separation that is inversely proportional to the square root of molecular weights ratio. Selective adsorption onto the pore surface, followed by surface diffusion of the adsorbed molecules, leads to the separation of the more strongly adsorbed component of a gas mixture and, hence, strongly depends on temperature. If partial condensation of some components of a gas mixture occurs in the pores, the exclusion and separation of the condensed molecule can be achieved. In separation, based on molecular sieving, molecules smaller than the pores will diffuse, whereas the larger molecules will be partially or completely obstructed.

Restricting ourselves to models for predicting transport rates through molecular sieves, we need to first consider the rate through a single pore, and then the rate through a pore network. Because the rate is extremely sensitive to pore diameter, the average flux in a pore network significantly differs from that predicted by a single pore. Because of a lack of information on the network properties, the focus is on the rate through a single pore; however, later we will try to predict the pore-size distribution. Determining the rate requires information on the energy associated with transition from the gas phase to the membrane (adsorption), and of a molecule hopping between the energy equilibrium minima inside the pore. However, we need to find the pre-exponential coefficients. Some simple expressions are described below. The rate coefficient for diffusion in a three-dimensional (3-D) solid lattice model is usually expressed as (Deen, 1998)

$$D = \frac{ul}{6} \exp\left(-\frac{\Delta G^*}{kT}\right)$$

where  $u$  is the molecule velocity,  $l$  is the lattice spacing, and  $\Delta G^*$  presents the difference between maximum and minimum free energies along the diffusion path. For diffusion in pores of radius  $r$ , it was suggested that

$$D = r \sqrt{\frac{8RT}{\pi M}} e^{-(\Delta E/RT)}$$

so that the expression is reduced to that of Knudsen diffusion when  $\Delta E$  is small. Knowing the energetics still poses the problem of how to describe the process in continuum models, the diffusion in many cases occurs as a single file and does not follow Einstein's or Fick's laws. The problem of diffusion of two or more components is still largely open. Several researchers (Acharya et al., 1997) have examined the driving force normalized flux, or permeance of various molecular probes through the membrane system. Strano and Foley (2000) and Acharya and Foley (2000) assumed that entropic effects dominated the transport through the membrane. Membrane permeance was best correlated to the minimum projected area of the molecule.

Molecular simulations provide a deeper understanding of the mechanisms of transport and separation through porous materials, and, hence, are playing an increasingly important role in the analysis of experimental data, and the molecular design of such materials. They are based on either equilibrium or non-equilibrium molecular dynamics (MD), or on Monte Carlo (MC) simulations (MacElroy et al., 2001; Demontis et al., 2001; Ohba and Kaneko, 2002; Tuzun et al., 1996, 1997; Ayappa, 1998). Adsorption and separation of hydrogen and other light gases in carbon nanotubes and in metal-intercalated nanotube bundle were modeled by Challa et al. (2001, 2002), Skoulidas et al. (2002), and by Simonyan and Johnson (2002). Skoulidas et al. (2002) predicted that the carbon nanotube membranes would have fluxes that are orders of magnitude greater than those in zeolite membranes. Xu et al. (1999, 2000) simulated the transport and separation characteristics of binary and ternary mixtures of  $H_2$ ,  $CO_2$  and  $CH_4$  through a slit shape carbon pore with nonequilibrium dynamic methods. Mao and Sinnott (2000) studied the flow of methane, ethane, and ethylene, through carbon nanotubes at room-temperature, with molecular dynamic simulations. Such theoretical methods, however, are limited to small systems and employ "predefined potentials" usually on the basis of empirical data on interaction of molecules with a planar surface. The full interaction is typically broken up into two-body, three-body, and many-body contributions, long-range, and short-range terms, and so on (Gray and Gubbins, 1984). Energy separation of this kind is rather murky in the case of such a sterically complex situation, such as a molecule inside a nanopore. To understand the transport and separation of gas mixtures in a carbon membrane, that consist of many interconnected pores, it must be first understood that the same phenomena is in a single carbon nanopore. In this work, we apply molecular mechanics (MM) modeling to determine the behavior and energetics of hydrogen, nitrogen, and  $C_1$ - $C_4$  hydrocarbon molecules inside cylindrical nanopores, modeled by short single-walled zigzag carbon nanotubes of various sizes. Energetic results obtained, are further used for the kinetic modeling of diffusion of individual molecules in nanotubes of each particular size. These kinetic

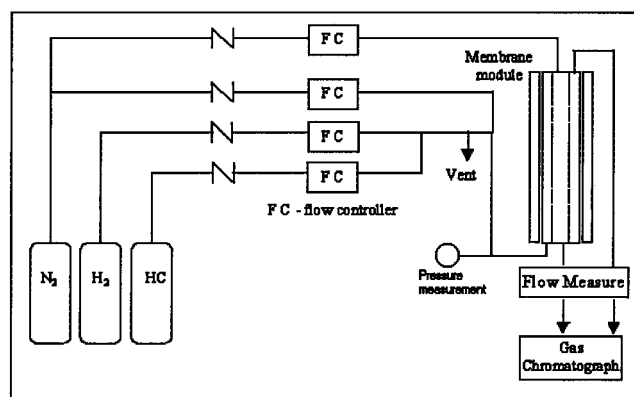


Figure 1. Permeation experimental system.

data are compared with the corresponding experimental values. The kinetic modeling of bi- and three-component diffusion is presented elsewhere, and also is briefly reviewed here.

The remainder of this work is organized as follows. The experimental methods and equipment are described in the following section. Obtained results, and the computation of the permeability factors, are outlined in the Experimental results section. In the section Molecular Mechanics Simulations, the method and results of simulations are presented. The Molecular diffusion inside nanopores subsection is devoted to the kinetic modeling of molecular transport inside nanopores, based on the MM results, and to contrasting the experimental data with theory.

## Experimental

The carbon membrane is a hollow fiber membrane, produced by Carbon Membranes, Ltd. (Temed Industrial Park, Israel). An entire membrane module, 30 cm length, composed of 100 fibers was used. The calculated membrane area for transport in this module is approximately  $150 \text{ cm}^2$ . The following gases were chosen as those with the potential for separation: hydrogen, methane, ethane, propane, normal- and isobutane. Nitrogen was used as an inert carrier gas, and to dilute and control the initial concentrations.

Permeation and selectivity studies were performed in an experimental system, as illustrated in Figure 1. The carbon membrane module was supplied as a tube and shell module, where the gases enter in the shell side, and the permeate exits through the tubes (carbon fibers). Single-component gases, or a mixture of hydrogen and hydrocarbon, entered the module in the shell side. The flow rate of the entering gases was set and measured by flow controllers. In the single-component systems, the driving force for gas transport through the membrane was the total pressure gradient, whereas in the binary systems the gas flow was achieved with nitrogen as a sweeping gas. Total stream flows and concentrations were measured at steady state. Based on or from these data, partial flows were calculated. The system worked at atmospheric pressure.

The membrane module was heated to the working temperature by heating elements fitted in a metal cover outside the module, and the entire module was thermally insulated. The temperature in the module was measured by a number of thermocouples, giving an isothermal behavior all over the

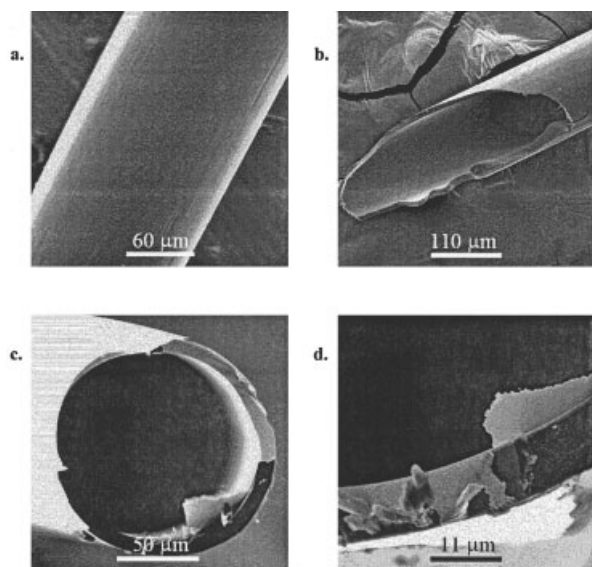


**Figure 2.** SEM micrographs of the carbon membrane fibers.

membrane. The carbon hollow fibers were supported in the module edges by epoxy glue, that is stable only up to 150°C. To overcome the overheating of the membrane sealing, a special cooler was built in each module edge.

Analysis of permeate and retentate composition was conducted by a (PerkinElmer Auto System XL) gas chromatograph, equipped with a thermal conductivity detector (TCD), for the organic compound measurements; a flame ionization detector (FID) for the inorganic compounds, and two types of packed columns for separation (8ft. 1/8 in. OD, SS column with Haysep Q 80/100 packing, and 7ft. 1/8 in. OD, SS column with 0.19% picric acid on Graphpac-GC 80/100 packing - Alltech). The flow rate of the exiting gases was measured by bubble columns. The permeation rate was calculated from the flow data. The effects of temperature, flow rate, and flow pattern of the sweeping gas on the permeation and selectivity were investigated.

Scanning electron microscopy (SEM) pictures were taken, after a coating with a gold layer to reduce high-energy beam damage, to characterize the carbon fiber membrane (Figure 2). The typical diameter of the carbon membrane fiber, which seems to be free of large cracks or pinholes, is found to be about 100  $\mu\text{m}$ , and the typical thickness of the carbon layer is approximately 10  $\mu\text{m}$ . The membrane is asymmetrical. No pores are seen in these micrographs, because of the low resolution that can be achieved in the SEM.

Surface areas (BET) and pore-size distribution were measured with a Micromeritics ASAP 2010 apparatus (Figure 3). Before adsorption measurements, the sample (approximately 150 mg) was outgassed at 573 K for 54 h. Most of the pore volume is made of 6 Å pores (diameter from nucleus to nucleus), whereas pores larger than 13 Å are practically absent (Figure 3).

## Experimental results

Single-component permeations were measured by applying a pressure gradient across the membrane at two temperatures (200

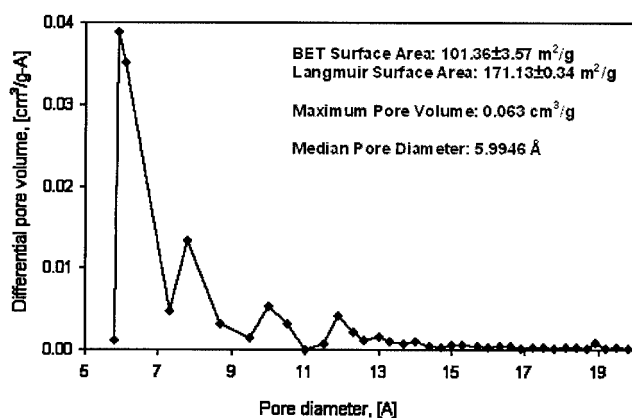


**Figure 3.** Pore size distribution obtained by BET measurements.

and 400°C) at steady state; the shell side pressure was kept atmospheric (Figure 4). For most gases, the fluxes are larger at higher temperature. The fluxes increase with the driving force, but not always linearly. Assuming a linear dependence, the permeabilities of the various components were calculated.

In a typical multicomponent experiment, a hydrogen and hydrocarbon (almost 1:1) mixture (or just hydrocarbon) was passed through the shell side, whereas nitrogen was the sweeping gas in the tube side flowing countercurrently. Both streams were at about atmospheric pressure. The modeled system is shown in Figure 5. To calculate membrane permeabilities, a mass balances model was written. The model makes the following assumptions: the system is isothermal and works at atmospheric pressure, the model is 1-D, plug flow applies on both sides, axial diffusion is negligible, and membrane permeabilities are constants all over the membrane. The last assumption may be questionable as multicomponent permeabilities (that is, in a hydrogen and hydrocarbon mixture) may significantly differ from those computed with a single component. In

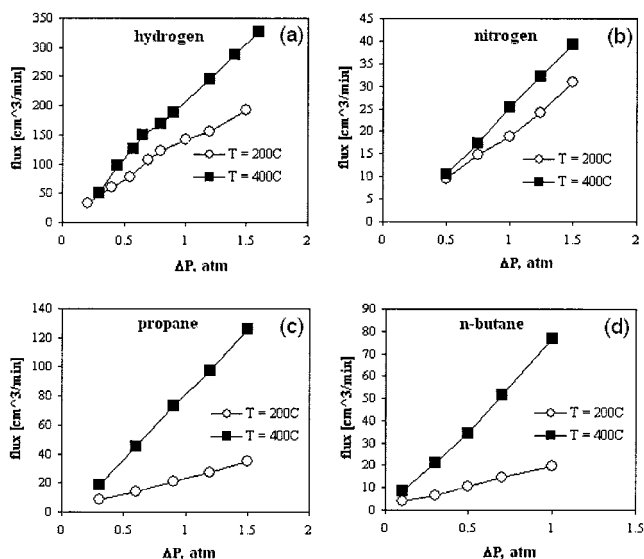


**Figure 4.** Single-component hydrogen (a) nitrogen (b) propane (c) and butane (d) fluxes driven by pressure gradient.



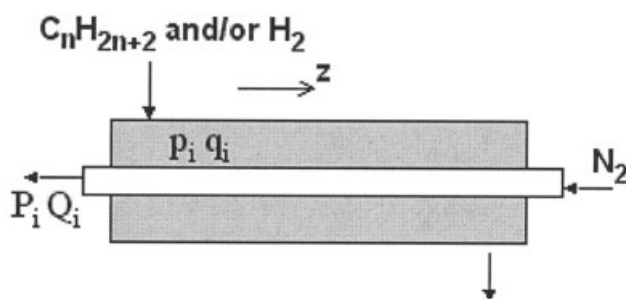


Figure 5. Membrane module for model calculations.

the absence of a solid theory, the calculated properties are averaged over all pore sizes, and over the concentration gradients employed.

The fluxes passing through the membrane are assumed linear with the driving force and then

$$\frac{dq_i}{dz} = sk_i(P_i - p_i) = -\frac{dQ_i}{dz} \quad (1)$$

where  $p_i$  and  $P_i$  denote the partial pressure (atm) of component  $i$  in the shell, and inner membrane side, respectively;  $q_i$  and  $Q_i$  are the corresponding partial flows ( $\text{cm}^3/\text{min}$ );  $s$  is the transport area perimeter (cm), and  $k_i$  is the membrane permeability for component  $i$  ( $\text{cm min}^{-1}\text{atm}^{-1}$ ). Because

$$\frac{dq_i}{dz} + \frac{dQ_i}{dz} = 0 \quad (2)$$

we can find from the measured inlet or outlet concentrations,  $q_i + Q_i = C_i$  constants that are invariant ( $z$ -independent). The partial pressures are calculated by the ratio of the single component flow by the total flow

$$P_i = \frac{Q_i}{\sum Q}; \quad p_i = \frac{q_i}{\sum q} \quad (3)$$

After substitution of partial pressures and constants, a set of differential equations are obtained. For example, in a system with  $C_i$  and  $H_2$  in the shell side, and  $N_2$  as sweeping gas

$$\frac{dq_{N_2}}{dz} = sk_{N_2} \left( \frac{C_1 - q_{N_2}}{C_1 + C_2 + C_3 - q_{N_2} - q_{H_2} - q_{C_i}} - \frac{q_{N_2}}{q_{N_2} + q_{H_2} + q_{C_i}} \right) \quad (4)$$

$$\frac{dq_{H_2}}{dz} = sk_{H_2} \left( \frac{C_2 - q_{H_2}}{C_1 + C_2 + C_3 - q_{N_2} - q_{H_2} - q_{C_i}} - \frac{q_{H_2}}{q_{N_2} + q_{H_2} + q_{C_i}} \right) \quad (5)$$

$$\frac{dq_{C_i}}{dz} = sk_{C_i} \left( \frac{C_3 - q_{C_i}}{C_1 + C_2 + C_3 - q_{N_2} - q_{H_2} - q_{C_i}} - \frac{q_{C_i}}{q_{N_2} + q_{H_2} + q_{C_i}} \right) \quad (6)$$

Using Matlab parameter estimation subroutines, and the experimentally determined concentrations and flows entering and exiting the membrane module, membrane constants were assessed. The initial guess of  $k_i$  for Matlab calculations was generated from the mean-log approximation

$$\frac{\Delta q_i}{\Delta z} = sk_i \frac{(P_i - p_i)_{in} - (P_i - p_i)_{out}}{\ln \left( \frac{(P_i - p_i)_{in}}{(P_i - p_i)_{out}} \right)} \quad (7)$$

Membrane permeabilities were calculated for each experimental system, and the flow profiles were plotted. Figure 6 presents, for example, the simulated shell-side partial flow profiles in a isobutane–hydrogen system. Membrane constants are collected in Table 1.

In all the systems, nitrogen passed through the membrane from the inner side to the shell side, and its concentration grew along the module. Hydrogen concentration decreased along the module, because of its transport through the membrane; all hydrocarbons (except of methane) concentrations remains almost constant along the membrane module, because of their small transport constants.  $H_2$  and  $N_2$  permeabilities ascend with the temperature, whereas hydrocarbon membrane permeabilities show no common behavior.

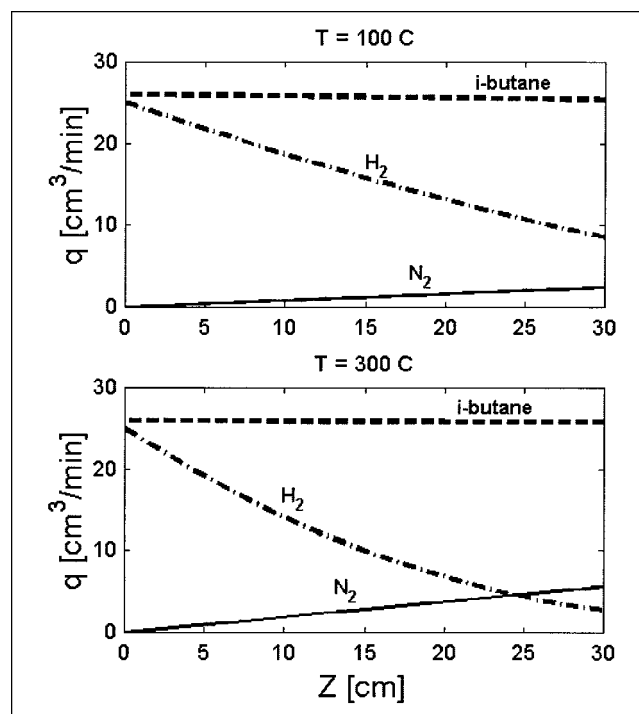


Figure 6. Shell side flow profiles in the *i*-butane–hydrogen system, with nitrogen as a sweeping gas at the module temperatures of 100 and 300°C.

**Table 1. Membrane Permeabilities ( $\text{cm} \cdot \text{min}^{-1} \cdot \text{atm}^{-1}$ ) in i-Butane-Hydrogen System Using  $\text{N}_2$  as a Sweeping Gas, as a Function of Module Temperature**

$T$ [ $^{\circ}\text{C}$ ]	$k_{\text{H}_2}$	$k_{\text{i-C}_4\text{H}_{10}}$	$k_{\text{N}_2}$
25	0.3185	0.0139	0.0247
100	0.5611	0.0102	0.0284
200	0.9802	0.0086	0.0533
300	1.1223	0.0032	0.0682
400	1.2336	0.0016	0.0749

Comparison of membrane permeabilities when propane is fed as an individual component, or as a mixture with hydrogen, both with sweeping nitrogen, shows that, in the latter mode (denoted as bi-component, Figure 7) the permeabilities are lower than those in the former mode (denoted as a single-component system). This is especially evident for propane permeability. It is even more evident when comparing these permeabilities with those determined under a pressure gradient (Figure 4,  $k_{\text{C}_3\text{H}_8} \sim 0.4 \text{ cm} \cdot \text{min}^{-1} \cdot \text{atm}^{-1}$  at  $400^{\circ}\text{C}$ ). This suggests that molecules of one component hinder the diffusion of the other molecules. The membrane permeabilities of hydrogen and nitrogen differ in different alkane mixtures, as demonstrated in Figure 8, for hydrogen. Hydrogen membrane constants ascend with the temperature in all the cases. Assuming an Arrhenius dependence, the activation energy ( $E_a/R$ ), and the pre-exponent ( $k_o$ ) were determined (Table 2).

Hydrogen membrane permeabilities are higher than all other constants (Figure 7). Hydrogen permeability declines somewhat as the size of the co-component molecule increases; ethane and propane inhibit the flux more than the other hydrocarbons (Figure 9a). The permeability of nitrogen, however, is significantly inhibited by the diffusion of  $\text{C}_2$  to  $\text{C}_4$  alkanes (Figure 9b), and is reduced by one order of magnitude, when compared to its permeabilities in methane.

Membrane selectivity factors were calculated for all the systems, and are summarized in Table 3. It can be seen that the selectivity values of hydrogen with propane, normal- and isobutane, in a multicomponent system, are very large at high temperatures (Table 3). Thus, carbon membranes should be

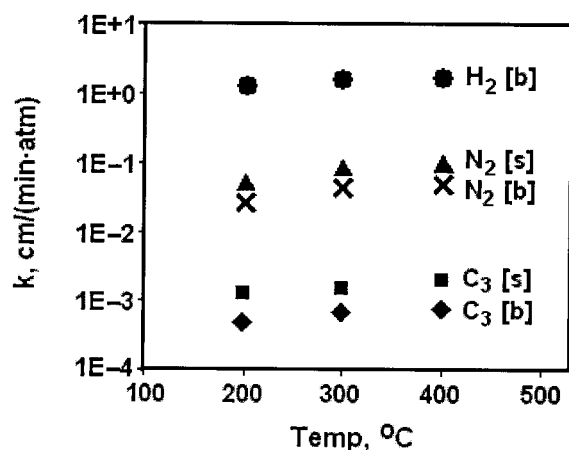


**Figure 7. Membrane permeabilities ( $\text{cm} \cdot \text{min}^{-1} \cdot \text{atm}^{-1}$ ) in the single-component propane (s), and in the bi-component propane–hydrogen (b) systems, both with nitrogen as a sweeping gas.**

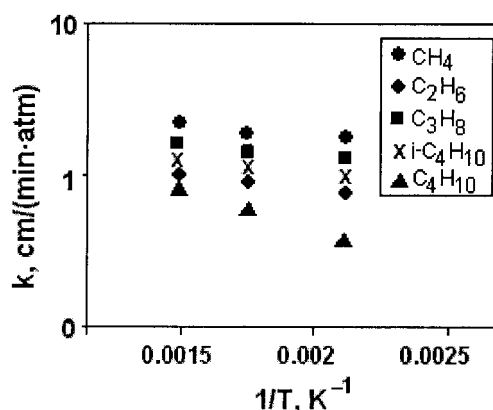


**Figure 8. Hydrogen permeabilities ( $\text{cm} \cdot \text{min}^{-1} \cdot \text{atm}^{-1}$ ) in the two-component hydrogen–hydrocarbon systems with nitrogen as sweeping gas, as a function of reverse module temperature.**

appropriate for carrying out a dehydrogenation reaction in a membrane reactor system. The permeabilities of  $\text{C}_2$  to  $\text{C}_4$  alkanes are also inhibited by the presence of nitrogen, and, thus, are reduced by 2–3 order of magnitude, when compared to their permeabilities as a single component transported under the pressure gradient (compare Table 3 to Figure 4; the selectivity is the ratio of slopes).

## Summary

Counterdiffusion of nitrogen, on one side of the membrane, and  $\text{C}_2$  to  $\text{C}_4$  alkanes with hydrogen, on the other side, significantly inhibits the fluxes of both nitrogen and alkanes, whereas hydrogen flux is only slightly diminished. Transport selectivities calculated from single-component data do not predict the behavior in the mixture.

## Molecular Mechanics Simulations

The dynamics of gases in systems with restricted geometry is known to be very different from that in the bulk (Gelb et al., 1999; Mon and Percus, 2002). The detailed mechanism of molecular transport in such systems is not fully understood yet. In this section, we present the results of molecular mechanics simulations that are aimed to provide microscopic details of the static and dynamic properties of the adsorbed molecules inside model cylindrical nanopores of various sizes.

## Computational details

Nanopores of various diameters were modeled by zigzag carbon nanotubes of varying size from (6,0) to (14,0), with C–C bond length of 1.42 Å. Such shape of carbon nanopores is consistent with the recent experimental data (Pfeifer et al.,

**Table 2. Activation Energy ( $E_a/R$ , K) and  $k_o$  ( $\text{cm} \cdot \text{min}^{-1} \cdot \text{atm}^{-1}$ ) for Hydrogen Membrane Permeabilities in Various Components Systems**

	$\text{CH}_4$	$\text{C}_2\text{H}_6$	$\text{C}_3\text{H}_8$	$\text{C}_4\text{H}_{10}$	$\text{i-C}_4\text{H}_{10}$
$E_a/R$	602.78	306.82	481.86	708.22	402.09
$k_o$	3.03	1.46	2.32	1.92	1.82

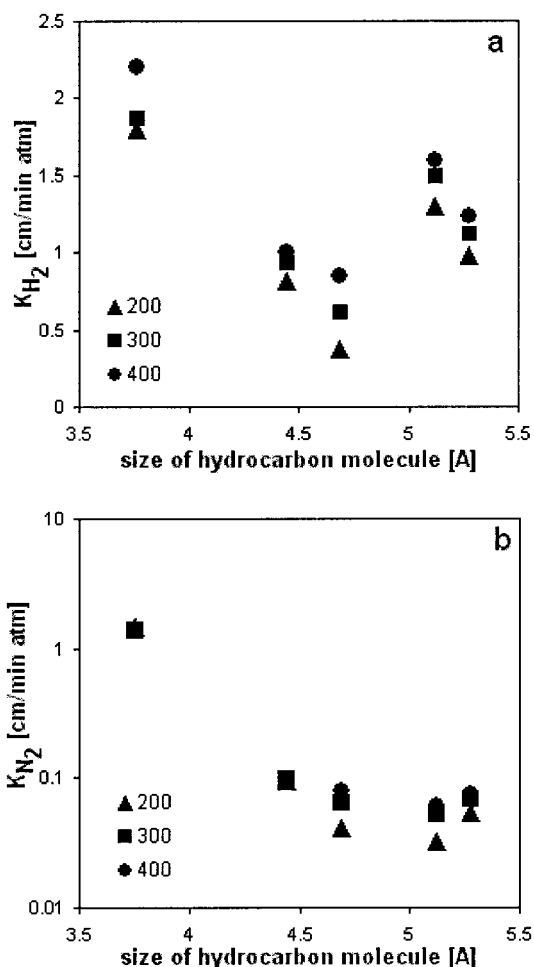


**Figure 9. Hydrogen (a) and nitrogen (b) permeabilities ( $\text{cm} \cdot \text{min}^{-1} \cdot \text{atm}^{-1}$ ) in the two-component hydrogen–hydrocarbon systems as a function of hydrocarbon size at the module temperatures of 200, 300 and 400°C.**

2002). These dimensions correspond to the pore size (D) from 4.3 to 11 Å or, considering carbon atoms as van der Waals spheres corrected by the Corey–Pauling factor, to inner pore diameter ( $d$ ) from 1.9 to 8.6 Å. These pore sizes are chosen based on the presented experimental results. The length of nanotubes were usually set to 11.4 Å (12 carbon layers), with outer C-atoms being saturated with hydrogen ( $d_{C-H} = 1.07$  Å). Removal of the saturating H-atoms causes a negligible ( $\sim 0.5\%$ ) decrease in the pore–molecule interaction energy. Figure 10 presents the (10,0) model nanotube as an example. In

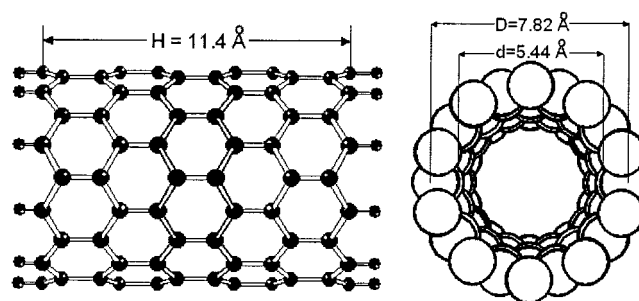


**Figure 10. Front and side views of the model zigzag nanotube (10,0) explaining the notations of length of nanotube (H), pore diameter (D), and inner-pore diameter (d), employed in this work.**

order to check the influence of the pore length on the energetics of pore–molecule interactions, several calculations were performed with a nanotube of 7.1 Å and 27.7 Å in length (8 and 32 carbon layers, respectively).

Movement of molecular species through the nanotubes was modeled by the relaxed potential energy surface (PES) scan with an optimized orientation of a molecule inside the nanotube, and allowed rotation of atoms around C–C bonds, whereas bond lengths and  $sp^3$  valence bond angles were fixed. The geometry of the nanotubes was frozen in all calculations. The energetic effect of the introduction of a molecule into a pore was calculated as the difference between the energy of the system with optimal position of a molecule inside a nanotube, and the energy of the corresponding separated components.

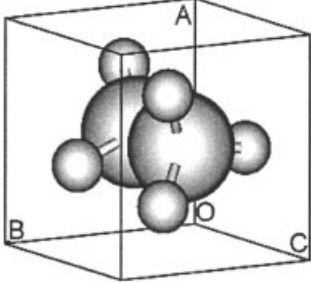
The computational approach applied for the molecular mechanics modeling was the universal force field (UFF) of Rappe et al. (1991, 1992), as it is implemented in the Gaussian 98 package (Frisch et al., 1998). Several PM3 calculations were performed to validate the UFF results. The electron density distribution on van der Waals spheres of atoms, and corresponding molecular sizes were obtained with Molden visualization software (Schaftenaar and Noordik, 2000).

The relationship between molecule size and the inner-pore diameter is critical for the separation efficiency of the membrane. Theoretical evaluations generally assume that molecules are solid spheres. The exact molecular dimensions of hydrogen, nitrogen hydrocarbons, based on the van der Waals radii, scaled by the Corey–Pauling factor, are listed in Table 4 in comparison with Lennard–Jones (LJ) diameters. It can be seen, for several molecules, that the spherical approximation is too crude. Moreover, the LJ diameter of the  $C_3H_8$  molecule is much larger than that of the  $C_4H_{10}$  molecule, and is almost as large as that of the  $i-C_4H_{10}$  molecule. Because of the nonuniform electron density distribution in the molecule, its representation as a distorted sphere is not satisfactory. Figure 11 illustrates the nonuniform electron density distribution along the shortest and longest dimensions in the two  $C_4$  isomers. Tortuosity in the electron density distribution on the carbon nanotube wall can also largely affect the energetics of a molecule interaction with the nanotube. Acharya and Foley (2000) considered the smallest dimension of a molecule ( $l_s$ ), as a limiting geometric factor that is consistent with a narrow slit shape of the pore. In the case of a cylindrical pore model, the intermediate

**Table 3. Selectivity Values, the Ratio of Hydrogen to Hydrocarbon Permeabilities, as a Function of Working Temperature**

$T$ [°C]	$\alpha_{H_2/CH_4}$	$\alpha_{H_2/C_2H_6}$	$\alpha_{H_2/C_3H_8}$	$\alpha_{H_2/C_4H_{10}}$	$\alpha_{H_2/i-C_4H_{10}}$
25	1.1	13.3	30.1	23.3	22.9
100	2.6	23.4	627.0	82.6	55.0
200	2.0	48.5	1625.0	291.3	114.0
300	2.8	57.3	1875.0	436.8	350.7
400	4.0	62.2	2000.0	941.6	771.0

**Table 4. Molecular Dimensions of Hydrogen, Nitrogen and C<sub>1</sub>—C<sub>4</sub> Hydrocarbon Molecules\* Based on Corey-Pauling Corrected van der Waals Radii in Comparison with Lennard-Jones Diameters**

	Molecule	OA = $l_1$	OB = $l_2$	OC = $l_3$	LJ
	H <sub>2</sub>	1.588	1.588	2.328	2.827
	N <sub>2</sub>	2.144	2.144	3.194	3.798
	CH <sub>4</sub>	3.367	3.643	3.768	3.758
	C <sub>2</sub> H <sub>6</sub>	3.640	3.643	3.855	4.443
	C <sub>3</sub> H <sub>8</sub>	3.368	4.648	5.506	5.118
	C <sub>4</sub> H <sub>10</sub>	3.637	4.842	5.921	4.687
	i-C <sub>4</sub> H <sub>10</sub>	5.124	5.199	5.478	5.278

\*All values are in Å. Notations are shown in the left column on the example of ethane molecule.

dimension ( $l_2$ ) will mainly determine the steric effects of the interaction. It is well known that individual groups in hydrocarbon molecules can freely rotate around C—C bond with formation of various conformers with very close stability. All these effects can be accurately represented in molecular mechanics methods, and are accounted for in our atomistic modeling.

Inside small nanopores, molecules optimize their positions to reduce the repulsion with pore walls. If the intermediate molecular dimension  $l_2$  is smaller than the pore diameter  $r$ , its longest axis ( $l_3$ ) is directed along the nanotube axis. With increasing pore size, the molecule “condensates” on the wall with  $l_2$ -axis being parallel to the wall to maximize the interaction. Only a hydrogen molecule is able to enter the smallest (6,0) nanotube, and even in this case, interaction is energetically strongly unfavorable. Therefore, this nanotube will not be considered for further discussion.

We considered the energetics of the two processes: the adsorption of a molecule inside a pore, that is, bringing the molecule into the pore mouth, or its desorption outside as a reverse process, and molecular transport within the pore.

### Pore–molecule interactions

For the first process, we found that the heat of introduction of a molecule into the nanotube varies with relative pore—molecule sizes: it is exothermic for  $l_2 < d$ , and is endothermic if the molecule is notably larger than the inner pore diameter ( $l_2 > d$ ) (Figure 12 and Table 5). Because the effect arises from the decrease of surface tension, the capillary energy increases with the contact surface. The largest dimension of a molecule ( $l_3$ ) plays the key role here. The strongest interaction takes place when the molecule size is close to the pore diameter ( $d \approx l_2$ ). The heat of interaction of a molecule with a cylindrical pore of a given size could be correlated in a form similar to the Lennard–Jones equation

$$\Delta H = 4\epsilon \left( \left( \frac{\sigma}{r^*} \right)^\alpha - \left( \frac{\sigma}{r^*} \right)^\beta \right) \quad (8)$$

where  $\epsilon$  is a constant,  $r^* = (d + 2.38)/2$  is the pore radius associated with the carbon atom positions, and  $\sigma$  is the pore radius at which the potential function changes its sign. In correlating the expression, we found that the length scale ( $\sigma$ ) linearly relates with the intermediate molecular dimension  $l_2$  as ( $\sigma = 0.3438 \cdot l_2 + 2.2319$ ;  $R^2 = 0.9321$ ; length in Å and energies in kcal/mol), whereas the energy scale ( $\epsilon$ ) is linear with the molecule “length”  $l_3$  ( $\epsilon = 0.25 \cdot l_3$ ;  $R^2 = 1.000$ ). Such relationships directly arise from the nature of the molecule–pore interaction, and was reported for interaction of alkanes with zeolites (see, for example, Bates and van Santen, 1998). In the shorter nanotubes, the pore–molecule interaction energies are slightly lower.

As expected, the interaction potential of a molecule with a cylindrical wall is stronger than that with micro- and mesopores of an activated carbon (see Table 5). The latter parameter presents, probably, the asymptotic value for the molecule–pore interaction energy with a surface (that is, large pore diameter). Isosteric heat of adsorption on carbon molecular sieves is higher than that on activated carbon, and the difference increases with the increasing size of the adsorbed molecule (Valenzuela and Myers, 1989; Groszek et al., 2002). For the activated carbon adsorbents, it was observed that the most effective micropores should be about 1.3 to 1.8 times larger in width than the kinetic diameter of the target adsorbate (Li et al., 2002).

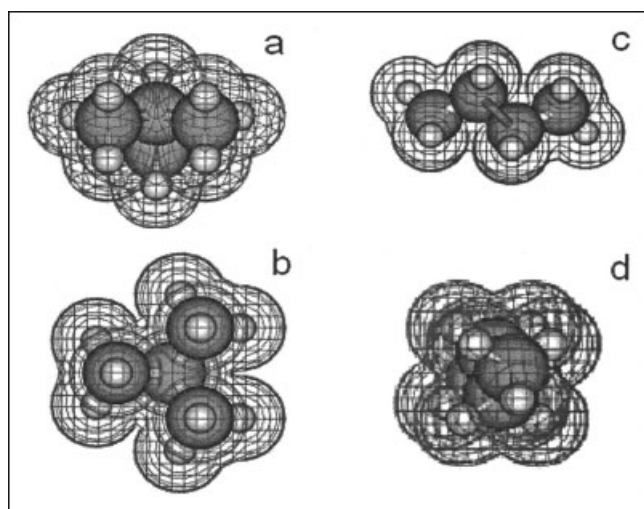


**Figure 11. Front and side views of the electron density distribution along van der Waals spheres in the *i*-butane (a, b) and *n*-butane (c, d) molecules.**



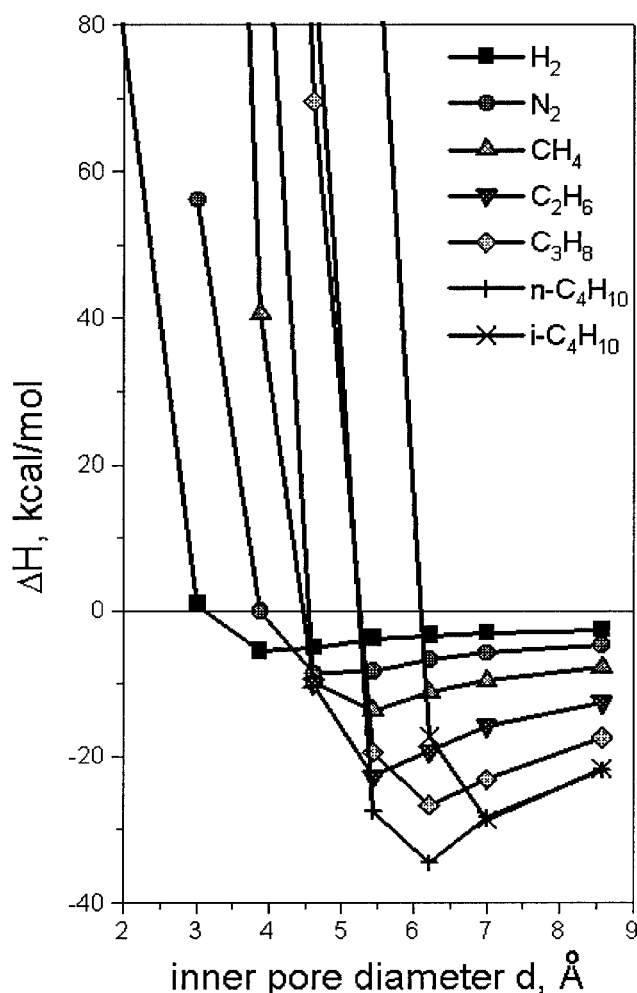


**Figure 12.** Pore-molecule interaction energy for hydrogen, nitrogen and C<sub>1</sub>-C<sub>4</sub> hydrocarbons as a function of inner-pore diameter.

### Molecular diffusion inside nanopores

The second process—diffusion of individual molecules inside nanopores—is again determined by the size difference of the pore and molecule. For  $l_2 \ll d$ , molecular movement along the

pore length is nonactivated. If the pore size is small as compared to the size of molecule  $l_2$ , the diffusion becomes activated. For a given molecule, the height of the barrier increases sharply with decreasing pore size, in the range where  $l_2 \approx d$ . Typical PES cross-section along the lowest energy diffusion pathway for activated diffusion is shown in Figure 13a, and the calculated activation barriers are collected in Table 6. Typical PES cross-sections for the capillary condensation regime are presented in Figure 13b. In the relatively short nanotubes, a molecule moves toward the center of the nanotube, with increasing energy gain, and with the most stable position of the molecule being at the pore center. If the pore length is much higher than the largest molecule dimension ( $H \gg l_3$ ), the pore-molecule interaction energy remains constant along the central part of the tube and decreases near the pore ends. It will be shown elsewhere that, moving along such pores, certain molecules follow a helical path with different convolution, allowing each point to maximize the pore-molecule interaction. Similar spiral paths of molecular motion were recently computed by molecular dynamics approach for ethane and ethylene molecules in (10,10), and (19,0) carbon nanotubes (Mao and Sinnott, 2002). As follows from the nature of the interaction, at distance  $l_3$  from the pore ends, the energy gain increases as a larger part of the molecule is located inside the pore. The long-range contributions, which determine the energetics of the interaction in the remainder of the nanotube length, do not exceed 10% of the total interaction energy.

### Influence of a second molecule on adsorption and diffusion inside a nanopore

The interaction of two molecules inside a nanotube was also checked for the coadsorption of a *n*-butane molecule, with any of the other molecules, inside the (11,0) nanotube of 12 carbon atoms in length. Initial results show that in the butane-hydrogen case, the strongly adsorbed butane molecule is located close to the center of the nanotube length, as in the case of a monocomponent system, whereas in the butane-propane system, the butane molecule is notably shifted to the pore end. However, the larger the second molecule is, the larger is the decline in the total adsorption energy, with respect to the adsorption energy of the individual components.

**Table 5.** Diameters of the Model ZigZag Nanotubes\* and the Maximal Energetic Effects (ΔH, kcal/mol) for Introduction of Individual Molecules into Zigzag Carbon Nanotubes of 11.4 Å in Length

Nanotube	(6, 0)	(7, 0)	(8, 0)	(9, 0)	(10, 0)	(11, 0)	(12, 0)	(14, 0)	AC**
<i>D</i> , Å	4.26	5.40	6.26	7.00	7.82	8.60	9.39	10.96	
<i>d<sub>v,dw</sub></i> , Å	0.86	2.00	2.86	3.60	4.42	5.20	5.99	7.56	
<i>d<sub>v,dw-CP</sub></i> , Å	1.88	3.02	3.88	4.62	5.44	6.22	7.01	8.58	
H <sub>2</sub>	87.5	0.8	-5.6	-5.2	-3.8	-3.4	-3.1	-2.7	-2.6
N <sub>2</sub>	—	56.1	-0.1	-8.6	-8.4	-6.8	-5.8	-4.7	-3.8
C <sub>1</sub> H <sub>4</sub>	—	—	40.6	-9.8	-13.7	-11.2	-9.6	-7.8	-4.4
C <sub>2</sub> H <sub>6</sub>	—	—	108.6	-10.1	-22.7	-19.3	-15.8	-12.6	-6.9
C <sub>3</sub> H <sub>8</sub>	—	—	—	69.6	-19.3	-26.6	-23.1	-17.4	-7.5
C <sub>4</sub> H <sub>10</sub>	—	—	—	88.0	-27.5	-34.6	-28.4	-21.9	-8.7
i-C <sub>4</sub> H <sub>10</sub>	—	—	—	—	100.4	-17.2	-28.7	-21.7	

\*See Figure 10 for notations.

\*\*Mean average isosteric heats of adsorption on different activated carbons at the limit of zero surface coverage, derived from the data of Valenzuela and Myers (1989).

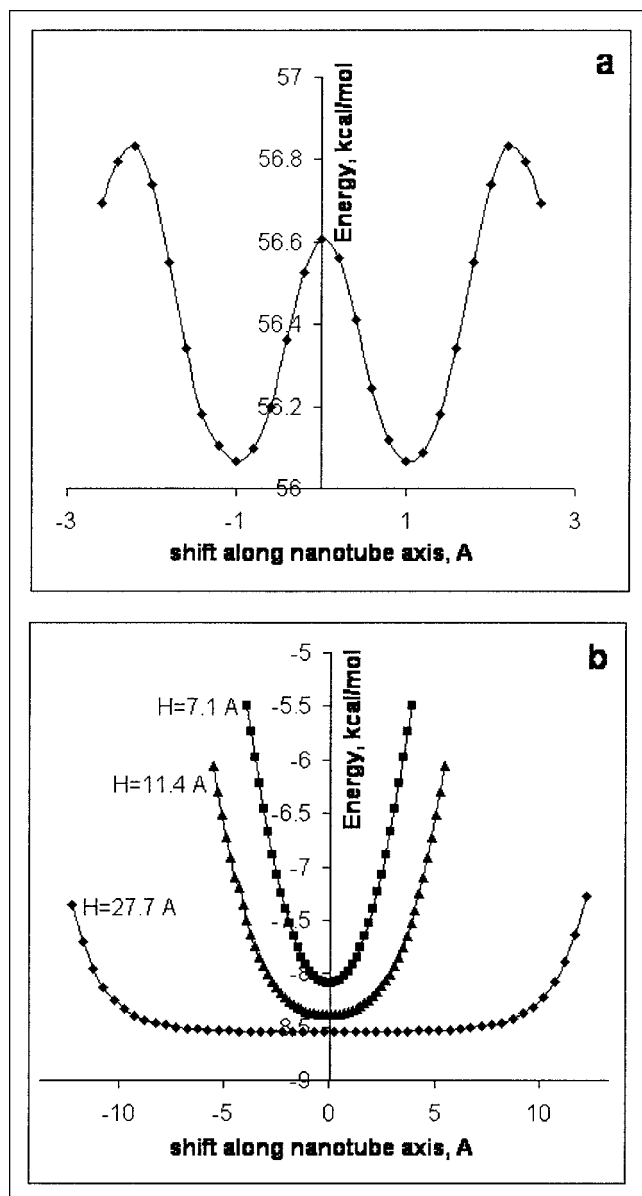


**Figure 13.** PES cross sections along the lowest energy diffusion pathway for activated diffusion of nitrogen molecule inside the (7,0) zigzag carbon nanotube of 11.4 Å in length (a), and for nonactivated nitrogen diffusion inside the (10,0) nanotubes of various lengths (b).

## Theory of Molecular Transport

Diffusion inside narrow pores can be classified as a single-file mode, where molecules are unable to pass each other (Sholl and Fichthorn, 1997); normal mode, where molecules are able to pass each other (Nelson and Auerbach, 1999), and an intermediate mode, that is referred to as the transition-mode diffusion (Sholl, 1999). The normal mode (viscous, molecular, or Knudsen) diffusion mechanisms are not relevant for nanopores smaller than 10 Å. The transition-mode diffusion in such pores is limited to two-layer, and only for small molecules in relatively large pores. The kinetics of the single-file transport in 1-D channels has attracted significant attention in recent years, with most applications for diffusion in zeolites (Jobic, 2000; Auerbach, 2000; Nelson and Auerbach, 1999; Wei et al., 2000; Wood et al., 2002). The molecular mechanics results reveal several unique features, which are not accounted for in most studies:

(1) The enthalpy of the pore-molecule interaction often can reach the energies of chemical bonding.

(2) There are three kinds of interactions inside cylindrical nanopores: (a) Endothermic pore-molecule interaction, with a high activation barrier for diffusion along the pore axis for  $l_2 > d$ ; this implies that the intermediate dimension of the molecule is larger than that of the pore, and the contribution of this mode to the flux is negligible; (b) exothermic pore-molecule interaction with a low activation barrier for diffusion when  $l_2 \approx d$ ; and (c) exothermic pore-molecule interaction with no diffusion barrier for  $l_2 < d$ .

(3) For the endothermic interactions (case a), the increase in total energy ( $\Delta H$  from Table 5) presents the activation barrier to the molecular adsorption in carbon nanopore, whereas Table 6 presents the activation barrier to molecular diffusion along the pore, and the desorption is nonactivated.

(4) For the exothermic interactions (case c), which present the most common situation, the adsorption is nonactivated as well as the diffusion inside the pore, whereas the desorption is a highly activated process with  $E_d = \Delta H$  (from Table 5). That results in a significant filling of the pores (capillary condensation). The desorption from a long pore should account for the interaction with a neighboring molecule, and for the fact that the energy of the outermost molecule location is not identical to that of a single molecule (that is, at the pore center).

To simplify the model we have made the following assumptions:

(1) Multilayer diffusion is neglected.

(2) In the lack of information on long-pore, many-molecule interaction, the outermost molecules are considered to have the same energy of interaction with the pore, as those in the pore

**Table 6.** Activation Barriers ( $E_a$ , kcal/mol) for the Diffusion of Individual Molecules Inside Model ZigZag Nanotubes

Nanotube	(6, 0)	(7, 0)	(8, 0)	(9, 0)	(10, 0)	(11, 0)	(12, 0)	(14, 0)
H <sub>2</sub>	9.4	1.0	0	0	0	0	0	0
N <sub>2</sub>	5.1	0.5	1.4	0	0	0	0	0
C <sub>1</sub> H <sub>4</sub>	—	19.1	0.7	0.2	0	0	0	0
C <sub>2</sub> H <sub>6</sub>	—	—	52.6	5.4	0.2	0	0	0
C <sub>3</sub> H <sub>8</sub>	—	—	—	8.7	0.65	0	0	0
C <sub>4</sub> H <sub>10</sub>	—	—	—	10.8	2.2	0	0	0
i-C <sub>4</sub> H <sub>10</sub>	—	—	—	—	15.8	2.9	0	0

Dashes stand here for the values larger than 100 kcal/mol.

center, that is, for the exothermic pore-molecule interaction, the activation barrier to desorption is set to  $E_d = \Delta H$ .

(3) The entropy factor is neglected, based on the small entropy changes accompanying pore molecule interactions reported by Acharya and Foley (2000), with respect to the heat effects obtained in our MM simulations.

Below, we show the derivation of the flux expression for a single-species transport from a reservoir at high-pressure on the left, to a low one on the right, with the above assumptions. The pressures of species  $i$  on the left and right sides, are denoted by  $P_l^i$  and  $P_r^i$ . We need to consider three steps—adsorption, diffusion and desorption. In the following section, the rates of these three steps are compared.

### Rates

The probability of a molecule  $i$  to enter a pore of size  $r_n = d/2$  from the gas phase is the adsorption flux ( $F^i$ ) multiplied by the cross section of the pore of interest ( $S_n$ ), multiplied by the probability of entry ( $W_{an}^i$ ). The flux, according to the Hertz–Knudsen equation, depends on the partial pressure of molecules  $P^i$ , their molecular mass  $m^i$ , and absolute temperature  $T$  as

$$F^i = P^i / (2\pi m^i k_B T)^{1/2} \quad (9)$$

where  $k_B$  is the Boltzmann constant. The probability of entry is

$$w_{an}^i = \chi_n^i \exp(-E_a/RT) \quad (10)$$

where  $R$  is the gas constant, and  $E_a$  the activation energy for adsorption, is  $\Delta H_n^i$  of the pore-molecule interaction (Table 5) if  $\Delta H > 0$ ; for most cases  $E_a = 0$ .

The  $\chi_n^i$  factor is the geometric probability of an ellipsoid molecule in an arbitrary distributed orientation, and with an arbitrary angle of incidence, to fit into the pore of diameter  $r_n$ . It has two contributions: the first is because of the angle of incidence with the plane, assuming sharp pore walls. This can be shown to be

$$\chi_n^i = 4 \int_0^{r_n - r_m} \arccos(r_m / (r_n - r)) r dr$$

for a spherical molecule of size  $r_m$  (sum average of  $l_2$  and  $l_3$ ). The second is the screening factor that applies for ellipsoid molecules ( $l_2 \neq l_3$ ), and shows a steep dependence on pore diameter when  $l_2 < r_n < l_3$ ; the latter will be ignored here. This whole approach assumes that adsorption occurs by impinging molecules. Another approach may assume adsorption on the outer membrane wall, and surface diffusion toward the pore mouth.

Combining the above equations yields the expression for the adsorption frequency of a molecule  $i$  inside a nanopore with inner diameter  $r_n$

$$R_n^i = \chi_n^i S_n P^i / (2\pi m^i k_B T)^{1/2} \exp(-E_a/RT) = k_{an}^i P^i \quad (11)$$

If adsorption is rate limiting, then the total flux is the sum over all pores of the difference between adsorption flux on the left ( $R_l^i$ ) and right ( $R_r^i$ )

$$J^i = \rho \sum_n (R_l^i - R_r^i) = \frac{\rho \Delta P^i}{\sqrt{2\pi m^i k_B T}} \sum_n a_n \chi_n^i S_n e^{(-E_d/RT)} \quad (12)$$

where  $\Delta P^i = P_l^i - P_r^i$ ;  $\rho$  is the total number of pores per unit of the membrane surface,  $a_n$  is the fraction of pores with diameter  $r_n$  normalized such that  $\sum_n a_n = 1$ .

The adsorption frequency ( $k_{an}^i$  at  $P=1$  atm) should be compared with that of desorption ( $k_{dn}^i$ ), and of transport ( $k_{tran n}^i$ ). The adsorption frequency of  $n$ -butane at 1 atm and 400°C, for which the flux is  $F=0.6 \cdot 10^{23}$  molecules/(cm<sup>2</sup> s), can be calculated to be  $2 \cdot 10^8$  s<sup>-1</sup> for a pore of 5.44 Å in diameter (with  $W_{an}^i=1$ ). And, thus, should be compared with the desorption frequency, which is an activated process with  $E_d = \Delta H_n^i$  and can be estimated from

$$k_{dn}^i = \frac{k_B T}{h} e^{(\Delta H/RT)}$$

to be  $1.7 \cdot 10^4$  s<sup>-1</sup> for the same conditions ( $h$  is the Planck constant). It is obvious, with very narrow pores or very large molecules, desorption is limiting the process.

Diffusion inside the pore is a complex process that can be described as a hopping of a molecule from site  $j$  to sites  $(j+1)$  and  $(j-1)$ , and back; the hopping frequency varies with the position near the edges, as well as the energy, where the hopping may be activated. Ignoring the former effect, and assuming a nonactivated transport (that is, a constant diffusivity) as calculated for most pores, the flux between the pore ends at the steady state is  $D\Delta P^i/(H\lambda)$ , where  $H=1 \mu$  is the estimate for the pore length (actually, the thickness of the selective carbon layer, as seen in Figure 2), and  $\lambda=2.1$  Å is the hopping distance. To estimate this term, we need to estimate diffusivity: if diffusion is treated as a chemical process, then  $D \sim (k_B T/h) \exp(-E_{tran}/RT) \lambda^2$  and the transport flux for  $\Delta P^i=1$  atm is  $k_{tran n}^i = (k_B T/h) \exp(-E_{tran}/RT) \lambda/H \sim 10^9$  s<sup>-1</sup>. For the same conditions described earlier, the diffusion is activated ( $E_{tran}=2.2$  kcal/mol, Table 6), and this transport frequency is reduced appropriately.

These order-of-magnitude calculations suggest that adsorption and transport, when it is not activated, are of similar magnitude (about  $5 \cdot 10^8$  s<sup>-1</sup>). Since  $k_B T/h \sim 10^{13}$  s<sup>-1</sup>, then desorption does limit the rate when  $(-\Delta H)/RT > 10$ , which translates to about  $(-\Delta H) > 10$  kcal/mol, that is, for large molecules, and pore sizes of  $d \approx l_2$  (Table 5). Calculation of  $k_a^i/k_d^i$  (Figure 14, with  $W_{an}^i=1$ , and at 1 atm.) reveals that in short pores, adsorption is limiting the transport of hydrogen and nitrogen, whereas desorption limits the transport of C<sub>2</sub> to C<sub>4</sub> alkanes in pores with inner diameter of 6–10 Å. Transport frequency will not affect the conclusion in the latter case, but it will affect the transport of nitrogen and hydrogen, and, thus, the pore length will become significant.

### Rate expressions

Before presenting the general solution of transport in a single nanotube pore, which is derived from a mean field approach, it

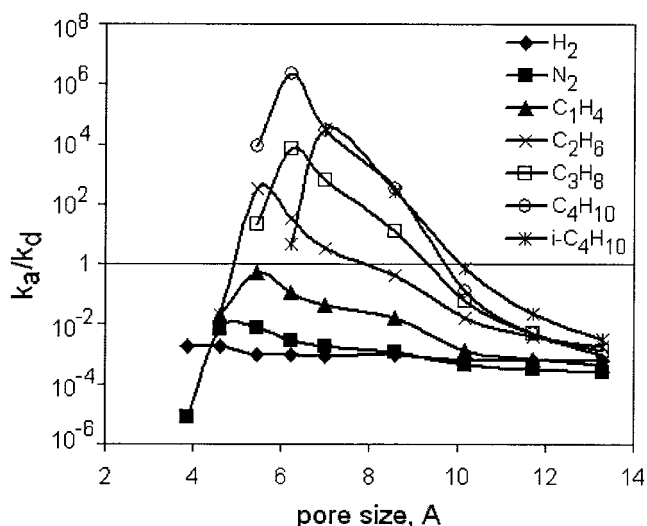


**Figure 14. Pore size dependence of the ratio of adsorption to desorption frequencies, for hydrogen, nitrogen, and C<sub>1</sub>–C<sub>4</sub> hydrocarbons at 1 atm.**

is important to derive the rate for the case that desorption is the rate-determining step, by considering the probabilities of the various steps. In that case, desorption can occur on the left or right side of the pore, and is followed instantaneously by adsorption, either on the left or on the right. If desorption occurred on the left, and adsorption on the right, then each molecule moves one step to the left, and we denote it as a leftward motion. The frequency of such leftward and rightward motions is  $M_l$ ,  $M_r$ . Now,  $M_{l,r} = (\text{frequency of left or right desorption}) \times (\text{probability of occupation on opposite side})$ . If desorption and adsorption occur at the same side, no motion can take place, however, the identity of the species may change.

For the simple situation described earlier, we can present the transport frequency ( $f$ ), number of transported molecules/time, as the difference of rightward and leftward motion

$$f = M_r - M_l$$

The frequency of desorption, either on left or right is  $k_{dn}^i$ , and the probability of occupation by adsorption on the left is  $P_l/(P_l + P_r)$ . Hence, when desorption is limiting

$$f_n^i = k_{dn}^i \left( \frac{P_l^i}{P_l^i + P_r^i} - \frac{P_r^i}{P_l^i + P_r^i} \right) = k_{dn}^i \frac{P_l^i - P_r^i}{P_l^i + P_r^i} \quad (13)$$

Thus, the flux is not linear with the gradient unless the gradient is very small. Note, that when  $P_r = 0$  (that is, under vacuum or high flow), the flux is  $f_n^i = k_{dn}^i$ .

We turn now to the general solution. The rates of adsorption, diffusion, and desorption should be equal at steady-state. Molecular motion in a single-file regime was shown to follow Fick's law (or rather, the flux is linear with the gradient). Writing a mean-field approach to the problem, we find

$$k_{an}^i P_l^i (1 - \pi_l) - k_{dn}^i \pi_l = k_{tran,n}^i (\pi_l - \pi_r) \\ = -(k_{an}^i P_r^i (1 - \pi_r) - k_{dn}^i \pi_r) \quad (14)$$

where  $\pi_l$  and  $\pi_r$  are the probabilities of occupations by a molecule of the leftmost and rightmost sites of the pore, whereas  $(1 - \pi_l)$  and  $(1 - \pi_r)$  are the probabilities that the corresponding sites are vacant.

In the general case, the solution of Eq. 13 is

$$\frac{k_{an}^i (P_l^i - P_r^i)}{f_n^i} = K_n^i (P_l^i + P_r^i) + 2 \\ + \frac{(K_n^i P_l^i + 1)(K_n^i P_r^i + 1)}{k_{tran,n}^i / k_{dn}^i}; \quad K_n^i = \frac{k_{an}^i}{k_{dn}^i} \quad (15)$$

which reduces to Eq. 13, when desorption is limiting ( $k_{dn}^i \ll k_{an}^i, k_{tran,n}^i$ ) and to  $f = k_{an}^i (P_l^i - P_r^i)/2$  when adsorption is limiting. When both processes are limiting, and transport is fast ( $\pi_l = \pi_r = \pi$ ), we solve Eq. 14 to find

$$\pi = \frac{k_{an}^i (P_l^i + P_r^i)}{2k_{dn}^i + k_{an}^i (P_l^i + P_r^i)}; \quad f_n^i = \frac{k_{an}^i (P_l^i - P_r^i)}{2 + \frac{k_{an}^i}{k_{dn}^i} (P_l^i + P_r^i)} \quad (16)$$

When transport is limiting, Eq. 14 reduces to  $k_{tran,n}^i (\pi_l - \pi_r)$ , where  $\pi$  follows the Langmuir adsorption isotherm on both sides,  $\pi = K_n^i P_i / (1 + K_n^i P_i)$ .

For a single-sized pore system, we can express the selectivity for each regime. The selectivity, traditionally defined as the ratio of permeabilities

$$S = \frac{f_2 / (P_{2l} - P_{2r})}{f_1 / (P_{1l} - P_{1r})}$$

will depend on the experiment and parameters. In diffusion of individual components under a pressure gradient, keeping the same pressures in both experiments

$$S_{\text{des, limited}} = \frac{k_{dn}^2}{k_{dn}^1}; \quad S_{\text{ads, limited}} = \frac{k_{an}^2}{k_{an}^1} = \frac{w_2}{w_1} \sqrt{\frac{M_1}{M_2}} \quad (17)$$

for both regimes. The measured flux in a system with pore-size distribution is

$$J = \rho \sum_n a_n \frac{f_n^i}{N_a} \\ = \frac{\rho}{N_a} \sum_n a_n \frac{P_l^i - P_r^i}{2 \left( \frac{P_l^i + P_r^i}{k_{dn}^i} + \frac{(K_n^i P_l^i + 1)(K_n^i P_r^i + 1)}{K_n^i k_{tran,n}^i} \right)} \quad (18)$$

## Applications

The experimental results cannot be accounted for by a system made of single-size pores; such a model will not explain the experimentally measured selectivity from the single-com-



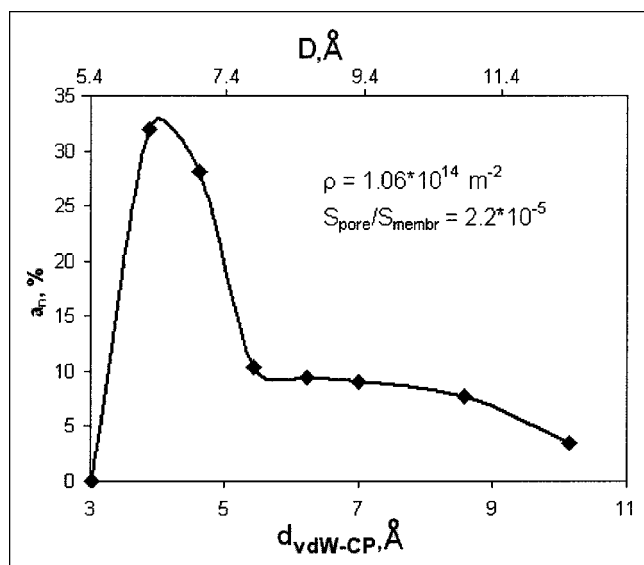


**Figure 15.** Pore size distribution obtained by fitting the parameters  $\rho$  and  $\alpha_n$  in Eq. 18, to the experimental pressure-driven fluxes through the membrane in single-component systems.

ponent data. The selectivity of adsorption-limited process (Eq. 17) varies mainly like the ratio of square root of molecular weights, and cannot account for the large  $S$  observations. Desorption-limited processes depend on the affinity, and  $S$  can vary significantly.

To test our theory, we computed the pore-size distribution by mean-square fitting of the total flux  $J$  (Eq. 18) to the experimental  $J$ – $\Delta P$  data, for the single-component systems (Figure 4, as well as  $\text{CH}_4$  and  $\text{C}_2\text{H}_6$ ). The obtained pore-size distribution (Figure 15) is in a good agreement with that measured by BET (Figure 3), that is, all pores are smaller than 13 Å and most pores are of 6–7 Å in size (measured from nucleus to nucleus, see upper  $x$ -axis scale in Figure 15).

The main observation of the experimental work is that counterdiffusion of nitrogen on one side of the membrane, and  $\text{C}_2$  to  $\text{C}_4$  alkanes with hydrogen on the other side, significantly inhibits the fluxes of both nitrogen and alkanes, whereas hydrogen flux is only slightly diminished. An analysis on the basis of a single-size pore cannot explain the dramatic change in permeabilities measured by counterdiffusion, and those measured as a single component. We need to consider the kinetics of codiffusion of hydrogen and alkanes, and counterdiffusion of nitrogen and alkanes. In a future publication, we will address these problems, however, we will review here the main results:

(1) Derivation of a flux expression for codiffusion of hydrogen and alkane molecules (or any two components) will show that in a desorption-limited process, the selectivity will differ from that derived here, however, the mutual effect is expected to be small.

(2) Derivation of the flux expression for counterdiffusion of two components, one from high pressure on the left to 0 on the right, and another from a high pressure on the right to 0 on the left, will be also considered. Especially, we want to determine whether both species diffuse, or just one, and, if so, which one? Its application to this system shows that, in desorption-limited

processes, each pore will be occupied by one species only, the one with the largest  $k_{a,n}^i P^i / k_{d,n}^i$  (see Figure 14). Let us consider the propane–nitrogen interaction, for example: because propane is larger (that is, smaller  $k_{a,n}^i$ ), but of a higher affinity to the pore (lower  $k_{d,n}^i$ ), this conclusion implies that the larger pores (yet, not large enough to violate the single-file diffusion) will convey the propane. In comparing fluxes and selectivities from single-component and counterdiffusion experiments, we note that there will be a range of pore diameters that are available for propane as a single component, and will be occupied by nitrogen in the latter experimentation mode, and vice versa. Thus, both propane and nitrogen permeabilities will decline.

(3) In this study, we neglected entropy changes accompanying molecule–pore interactions considering low entropy-change values calculated by Acharya and Foley (2000), for the hard-sphere model. Accounting for the capillary forces and for the inner molecular degrees of freedom could significantly influence the resulting pre-exponential coefficients of desorption, as will be shown in a later publication.

## Conclusions

This research is part of an effort to develop a carbon membrane reactor for dehydrogenation reactions. Carbon membranes are less expensive than the completely selective Pd membrane, and are significantly more selective than porous ceramics. The transport and separation of hydrogen and light hydrocarbons are studied in a molecular-sieve carbon membrane hollow-fiber module, at the temperature range of 25–400°C; nitrogen is used as a sweeping gas in the study of mixtures, and the fluxes of pure components are studied under a pressure gradient. The membrane selectivity, the ratio of hydrogen to hydrocarbon permeabilities, may reach 100 to 1,000 in propane, or in (normal or iso-) butane mixtures with hydrogen, making the membrane an excellent candidate for a membrane dehydrogenation reactor. The performance of the membrane reactor is presented elsewhere.

Reactor design requires information on the transport laws of the various components. Such information is missing for molecular sieve membranes, which are typically characterized by single-file diffusion. It is not clear whether the permeabilities are constants along the reactor, and how they change with composition. The permeabilities measured here in pure-component studies differ from those in mixtures. The main experimental observation is that counterdiffusion of nitrogen on one side of the membrane, and  $\text{C}_2$  to  $\text{C}_4$  alkanes with hydrogen on the other side, significantly inhibits the fluxes of both nitrogen and alkanes, whereas hydrogen flux is only slightly diminished. This results from the strong adsorption (or condensation) of hydrocarbons in the small pores. This is a significant and desired result from the reactor design perspective, because we are interested in a membrane that is selective to hydrogen transport.

To account for these results, we use molecular mechanics simulations to find the energetics of adsorption, diffusion, and desorption of individual gases in cylindrical nanopores, modeled by carbon nanotubes. In pore sizes that are up to 2–3 times the dimension of the molecule, diffusion of the molecule inside the pore is nonactivated, whereas desorption is activated, and is typically the rate limiting step for  $\text{C}_2$  to  $\text{C}_4$  alkanes; the mo-

molecular transport proceeds essentially by a single-file diffusion mechanism.

A rate expression for a single-species transport in a molecular-sieve carbon membrane is derived by mean-field approach. The pore-size distribution is calculated by comparing experimental and computational data. The results of co- or counterdiffusion in a two-component system are reviewed. Counterdiffusion of alkane and nitrogen results in a competition between the two on pores to convey them; whereas the alkane conquer most of the pores, which explains the decline in nitrogen transport, its own diffusion is also diminished because of masking of the other side by nitrogen. In the future, we will try to quantitatively verify this conjecture.

## Acknowledgments

The research was supported by The Ministry of Science, State of Israel. The BET and pore size distribution measurements were performed by Dr. Yu. Shindler. The authors thank Dr. I. Kaganov for useful discussion. Irena Efremenko would like to thank the Center for Absorption in Science, Ministry of Immigrant Absorption for partial financial support.

## Literature Cited

- Acharya, M., and H. C. Foley, "Transport in Nanoporous Carbon Membranes: Experiments and Analysis," *AIChE J.*, **46**, 911 (2000).
- Acharya, M., B. A. Raich, H. C. Foley, M. P. Harold, and J. J. Lerou, "Metal Supported Carbogenic Molecular Sieve Membranes: Synthesis and Applications," *Ind. Eng. Chem. Res.*, **36**, 2924 (1997).
- Auerbach, S. M., "Theory and Simulation of Jump Dynamics, Diffusion and Phase Equilibrium in Nanopores," *Int. Rev. Phys. Chem.*, **19**, 155 (2000).
- Ayappa, K. G., "Simulations of Binary Mixture Adsorption in Carbon Nanotubes: Transitions in Adsorbed Fluid Composition," *Langmuir*, **14**, 880 (1998).
- Bates, S. P., and R. A. van Santen, "The Molecular Basis of Zeolite Catalysis: A Review of Theoretical Simulations," *Adv. Catal.*, **42**, 1 (1998).
- Bird, A. J., and D. L. Trimm, "Carbon Molecular Sieves Used in Gas Separation Membranes," *Carbon*, **21**, 177 (1983).
- Burggraaf, A. J., and K. Keizer, *Inorganic Membranes Synthesis Characteristics and Applications*, R. R. Bhave, ed., Chapman & Hall, London, pp 10–63 (1991).
- Challa, S. R., D. S. Sholl, and J. K. Johnson, "Light Isotope Separation in Carbon Nanotubes Through Quantum Molecular Sieving," *Phys. Rev.*, **B 63**, 245419 (2001).
- Challa, S. R., D. S. Sholl, and J. K. Johnson, "Adsorption and Separation of Hydrogen Isotopes in Carbon Nanotubes: Multicomponent Grand Canonical Monte Carlo Simulations," *J. Chem. Phys.*, **116**, 814 (2002).
- Chen, N. Y., T. F. Degnan, and C. M. Smith, "Molecular Transport and Reaction in Zeolites," VCH Publishers, New York (1994).
- Deen, W. M., *Analysis of Transport Phenomena*, Oxford University Press, New York (1998).
- Demontis, P., J. G. Gonzalez, G. B. Suffritti, and A. Tilocca, "Statics and Dynamics of Ethane Molecules in AlPO<sub>4</sub>-5: A Molecular Dynamics Simulation Study," *J. Amer. Chem. Soc.*, **123**, 5069 (2001).
- Duren, T., and F. J. Keil, "Molecular Modeling of Adsorption in Carbon Nanotubes," *Chem. Eng. Technol.*, **24**, 698 (2001).
- Gelb, L. D., K. E. Gubbins, R. Radhakrishnan, and M. Sliwinski-Bartkowiak, "Phase Separation in Confined Systems," *Rep. Prog. Phys.*, **62**, 1573 (1999).
- Gray, C. G., and K. E. Gubbins, *Theory of Molecular Fluids*, Vol. 1, Clarendon, Oxford, U.K. (1984).
- Groszek, A. J., I. Avraham, A. Danon, and J. E. Koresh, "Interaction of O<sub>2</sub>, N<sub>2</sub> and He at room Temperature with Carbon Molecular Sieves Sensed by Adsorption Measurements," *Colloids and Surf. A*, **208**, 65 (2002).
- Jobic, H., "Diffusion Studies Using Quasi-Elastic Neutron Scattering," *Membr. Sci. Technol. Ser.*, **6**, 109 (2000).
- Keil, F. J., "Diffusion and Reaction in Porous Networks," *Cat. Today*, **53**, 245 (1999).
- Keil, F. J., "Modeling of Phenomena Within Catalyst Particles," *Chem. Eng. Sci.*, **51**, 1543 (1996).
- Khan, I. A., and K. G. Ayappa, "Density Distributions of Diatoms in Carbon Nanotubes: A Grand Canonical Monte Carlo Study," *J. Phys. Chem.*, **109**, 4576 (1998).
- Koresh, J., and A. Soffer, "Mechanism of Permeation Through Molecular Sieve Carbon Membrane. Part I. The effect of Adsorption and the Dependence on Pressure," *J. Chem. Sci. Faraday Trans. I*, **82**, 2057 (1986).
- Koresh, J., and A. Soffer, "Study of Molecular Sieve Carbons", Part 1. *J. Chem. Sci. Faraday Trans. I*, **76**, 2457 (1980).
- Koresh, J., and A. Soffer, "The Carbon Molecular Sieve Membranes. General Properties and the Permeability of CH<sub>4</sub>/H<sub>2</sub> Mixture," *Sep. Sci. Technol.*, **22**, 973 (1987).
- Koresh, J., and A. Soffer, "Molecular Sieve Carbon Permselective Membrane," Part 1 "Presentation of a New Device for Gas Mixture Separation", *Sep. Sci. Technol.*, **18**, 723 (1983).
- Kusuki, Y., H. Shimazaki, N. Tanihara, S. Nakanishi, and T. Yoshinaga, "Gas Permeation and Characterization of Asymmetric Polyimide Hollow Fiber Membrane," *J. Membr. Sci.*, **134**, 245 (1997).
- Li, L., P. A. Quinlivan, and D. R. U. Knappe, "Effects of Activated Carbon Surface Chemistry and Pore Structure on the Adsorption of Organic Contaminants from Aqueous Solution," *Carbon*, **40**, 2085 (2002).
- Frisch, M. J., G. W. Trucks, H. B. Schlegel, G. E. Scuseria, M. A. Robb, J. R. Cheeseman, V. G. Zakrzewski, J. A. Montgomery, Jr., R. E. Stratmann, J. C. Burant, S. Dapprich, J. M. Millam, A. D. Daniels, K. N. Kudin, M. C. Strain, O. Farkas, J. Tomasi, V. Barone, M. Cossi, R. Cammi, B. Mennucci, C. Pomelli, C. Adamo, S. Clifford, J. Ochterski, G. A. Petersson, P. Y. Ayala, Q. Cui, K. Morokuma, D. K. Malick, A. D. Rabuck, K. Raghavachari, J. B. Foresman, J. Cioslowski, J. V. Ortiz, A. G. Baboul, B. B. Stefanov, G. Liu, A. Liashenko, P. Piskorz, I. Komaromi, R. Gomperts, R. L. Martin, D. J. Fox, T. Keith, M. A. Al-Laham, C. Y. Peng, A. Nanayakkara, C. Gonzalez, M. Challacombe, P. M. W. Gill, B. Johnson, W. Chen, M. W. Wong, J. L. Andres, C. Gonzalez, M. Head-Gordon, E. S. Replogle, and J. A. Pople, "Gaussian 98, Revision A.7," Gaussian, Inc., Pittsburgh PA (1998).
- MacElroy, J. M. D., and S.-H. Suh, "Equilibrium and Nonequilibrium Molecular Dynamics Studies of Diffusion in Model One-Dimensional Micropores," *Microporous and Mesoporous Mat.*, **48**, 195 (2001).
- Mao, Z., and S.B. Sinnott, "A Computational Study of Molecular Diffusion and Dynamic Flow Through Carbon Nanotubes," *J. Phys. Chem.*, **104**, 4618 (2000).
- Mao, Z., and S. B. Sinnott, "Separation of Organic Molecular Mixtures in Carbon Nanotubes and Bundles: Molecular Dynamics Simulations," *Phys. Chem.*, **B, 105**, 6916 (2001).
- Mao, Z., and S. B. Sinnott, "Predictions of a Spiral Diffusion Path for Nonspherical Organic Molecules in Carbon Nanotubes," *Phys. Rev. Lett.*, **89**, 278301 (2002).
- Mon, K. K., and J. K. Percus, "Self-Diffusion of Fluids in Narrow Cylindrical Pores," *J. Chem. Phys.*, **117**, 2289 (2002).
- Nelson, P. H., and S. M. Auerbach, "Self-Diffusion in Single-File Zeolite Membranes is Fickian at Long Times," *J. Chem. Phys.*, **110**, 9235 (1999).
- Ohba, T. and K. J. Kaneko, "Internal Surface Area Evaluation of Carbon Nanotube with GCMC Simulation-Assisted N<sub>2</sub> Adsorption," *Phys. Chem.*, **B, 106**, 7171 (2002).
- Pfeifer, P., F. Ehrburger-Dolle, T. P. Rieker, M. T. Gonzalez, W. P. Hoffman, M. Molina-Sabio, F. Rodriguez-Reinoso, P. W. Schmidt, and D. J. Voss, "Nearly Space-Filling Fractal Networks of Carbon Nanopores," *Phys. Rev. Lett.*, **88**, 115502/1 (2002).
- Rao, M. B., and S. Sircar, "Nanoporous Carbon Membranes for Separation of Gas Mixtures by Selective Surface Flow," *J. Membr. Sci.*, **85**, 253 (1993).
- Rappe, A. K., and W. A. Goddard, "Charge Equilibration for Molecular Dynamics Simulations," *J. Phys. Chem.*, **95**, 3358 (1991).
- Rappe, A. K., C. J. Casewit, K. S. Colwell, W. A. Goddard, W. M. Skiff, "UFF, A Full Periodic Table Force Field for Molecular Mechanics and Molecular Dynamics Simulations," *J. Am. Chem. Soc.*, **114**, 10024 (1992).
- Saracco, G., and V. Specchia, "Catalytic Inorganic Membrane Reactors: Present Experience and Future Opportunities," *Cat. Rev. Sci. Eng.*, **36**, 305 (1994).
- Saracco, G., and V. Specchia, *Structured Catalysis and Reactors*, A.

- Cybulski and J. A. Moulijn ed., Marcel-Dekker, New York, pp. 463–500 (1998).
- Schaftenaar, G., and J. H. Noordik, "Molden: a Pre- and Post-Processing Program for Molecular and Electronic Structures," *J. Comput.-Aided Mol. Design*, **14**, 123 (2000).
- Sholl, D. S., "Characterizing Adsorbate Passage in Molecular Sieve Pores," *Chem. Eng. J.*, **74**, 25 (1999).
- Sholl, D. S., and K. A. Fichthorn, "Normal, Single-File, and Dual-Mode Diffusion of Binary Adsorbate Mixtures in AlPO<sub>4</sub>-5," *J. Chem. Phys.*, **107**, 4394 (1997).
- Skoulidas, A. I., D. M. Ackerman, J. K. Johnson, and D. S. Sholl, "Rapid Transport of Gases in Carbon Nanotubes," *Phys. Rev. Lett.*, **89**, 185901 (2002).
- Simonyan, V. V., and J. K. Johnson, "Hydrogen Storage in Carbon Nanotubes and Graphitic Nanofibers," *J. Alloys & Compounds*, **330**, 659 (2002).
- Sircar, S., M. B. Rao, and C. M. A. Thaeron, "Selective Surface Flow Membrane for Gas Separation," *Sep. Sci. Technol.*, **34**, 2081 (1999).
- Strano, M. S., and H. C. Foley, "Deconvolution of Permeance in Supported Nanoporous Membranes," *AIChE J.*, **46**, 651 (2000).
- Tanihara, N., H. Shimazaki, Y. Hirayama, S. Nakanishi, T. Yoshinaga, and Y. Kusuki, "Gas Permeation Properties of Asymmetric Carbon Hollow Fiber Membranes Prepared From Asymmetric Polyimide Hollow Fiber," *J. Membr. Sci.*, **169**, 179 (1999).
- Tuzun, R. E., D. W. Noid, B. G. Sumpter, and R. C. Merkle, "Dynamics of Fluid Flow Inside Carbon Nanotubes," *Nanotechnology*, **7**, 241 (1996).
- Tuzun, R. E., D. W. Noid, B. G. Sumpter, and R. C. Merkle, "Dynamics of He/C<sub>60</sub> Flow inside Carbon Nanotubes," *Nanotechnology*, **8**, 112 (1997).
- Uhlhorn, R. J. R., and A. J. Burggraaf, *Inorganic Membranes Synthesis Characteristics and Application*, R.R. Bhave, ed., Chapman & Hall, London, U.K., pp. 155–176 (1991).
- Valenzuela, D. P., and A. L. Myers, *Adsorption Equilibrium Data Handbook*, Prentice Hall, Englewood Cliffs, NJ (1989).
- Wei, Q.-H., C. Bechinger, and P. Leiderer, "Single-File Diffusion of Colloids in One-Dimensional Channels," *Science* (Washington DC), **287**, 625 (2000).
- Weitkamp, J., G. Olhamnn, J. C. Vedrine, and P. A. Jacobs, *Catalysis and Adsorption by Zeolites*, Elsevier, Amsterdam (1991).
- Wood J., L. F. Gladden, and F. J. Keil, "Modeling Diffusion and Reaction Accompanied by Capillary Condensation Using Three-Dimensional Pore Networks. Part 2. Dusty Gas Model and General Reaction Kinetics," *Chem. Eng. Sci.*, **57**, 3047 (2002).
- Xu, L., T. T. Tsotsis, and M. Sahimi, "Nonequilibrium Molecular Dynamics Simulation of Transport and Separation of Gases in Carbon Nanopores. Part I. Basic results," *J. Chem. Phys.*, **111**, 3252 (1999).
- Xu, L., M. G. Sedigh, T. T. Tsotsis, and M. Sahimi, "Nonequilibrium Molecular Dynamics Simulation of Transport and Separation of Gases in Carbon Nanopores. Part II. Binary and Ternary Mixtures and Comparison with the Experimental Data," *J. Chem. Phys.*, **112**, 910 (2000).

Manuscript received Feb. 23, 2003, and final revision received July 3, 2003